Electronic Supplementary Information

Disparate reactivity of a chiral Iron(II) tetracarbene complex with organic azides

Jerred J. Russell,[a] Joseph F. DeJesus,[a] Brett A. Smith,[a] Phattananawee Nalaoh,[a] Konstantinos D. Vogiatzis, [a,*] and David M. Jenkins,[a,*]

Department of Chemistry, The University of Tennessee,

Knoxville, Tennessee 37996, USA

Table of Contents

Experimental section

General Considerations for Synthesis

All reactions, workups and manipulations involving the NHC metal complexes and subsequent reactions were done using standard Schlenk techniques under N_2 or in an MBraun Unilab glovebox under N_2 unless otherwise stated. All glassware for aforementioned reactions were dried at 170 °C overnight before use. For air sensitive reactions, tetrahydrofuran (THF) and ^{n}hexane were dried on an Innovative Technologies Pure Solv MD-7 Solvent Purification System, degassed by three freeze-pump-thaw cycles on a Schlenk line, and subsequently stored under activated 4 Å molecular sieves prior to use. Benzene and pentane were purchased anhydrous from Sigma-Aldrich, degassed by three freeze-pump-thaw cycles and subsequently stored over activated 4 Å molecular sieves prior to use. For anhydrous NMR solvents, benzene-d_6 (C_6D_6), was degassed by three freeze-pump-thaw cycles and subsequently stored over activated 4 Å molecular sieves prior to use. Celite used in the purification of metal complexes was dried overnight at 240 °C and subsequently stored in the glovebox prior to use. All reagents were purchased from commercial vendors at highest purity. Octyl azide,[1] *tert*-butyl azide,[2] mesityl azide,[3] and *p*-tolyl azide[4] were synthesized from previously reported procedures. These azides were degassed by either sparging with N_2 for 30 minutes or by three freeze-pump-thaw cycles and stored over activated 4 Å molecular sieves. [($^{(S,S)\text{-}1,2\text{-}Cy,BMe}_2$TC^{H})Fe] (**1**) was also synthesized in the manner reported previously by our group.[5]

General Considerations for Molecular Characterization

Solution ^{1}H NMR and ^{13}C{^{1}H} NMR were performed on a Varian VNMRS 500 MHz narrow-bore broadband system at 298 K. All ^{1}H and ^{13}C shifts were referenced to the residual solvent. All mass spectrometry analyses were conducted at the Biological and Small Molecule Mass Spectrometry Center located in the Department of Chemistry at the University of Tennessee. The ESI-MS analyses were performed via direct infusion into a Waters Synapt G2-Si mass spectrometer. LDI-MS Samples were run on a Waters Synapt G2-Si MALDI mass spectrometer with a quadrupole time-of-flight mass analyzer. Samples were prepared by spotting directly onto the target plate (aluminum) without the addition of matrix. Infrared spectra were collected on a Thermo Scientific Nicolet iS10 with a Smart iTR accessory for attenuated total reflectance (ATR) using pure samples of each complex. UV-vis measurements were taken inside a dry glovebox on an Ocean Optics USB4000 UV-vis system with 1 cm path length quartz crystal cell. Solution magnetic moments were measured by the Evans method and were adjusted for diamagnetic contributions using the constitutive corrections of Pascal's constants. Evans method measurements were taken on a Varian 500 MHz NMR using an inner tube filled with C_6D_6.

General Considerations for Crystallography

All X-ray data collections were performed on single crystals coated in Paratone oil on glass slides and mounted on nylon fibers. X-ray data for complexes (**2**, **3**, **4**, **5**) were collected with the use of a Mo or Cu microsource on a Bruker D8 Venture diffractometer. Crystals were mounted in a 100 K cold stream provided by an Oxford Cryostream low-temperature apparatus. All data sets were reduced with Bruker SAINT and were corrected for absorption using SADABS. Structures were solved and refined using OLEX2, SHELXT and SHELXLE64, respectively.

General Considerations of Electrochemical Studies

Cyclic voltammetry measurements were made inside a dry glovebox at ambient temperature using a BASi Epsilon electrochemical analyzer with a platinum working electrode, platinum wire counter electrode, and $Ag/AgNO_3$ reference electrode. For all samples, a 0.1 M solution tetrabutylammonium hexafluorophosphate ($(TBA)(PF_6)$) in the appropriate solvent was used as the supporting electrolyte. All peaks were referenced to an external standard of ferrocene. Unless overwise stated, all experiments were initiated at more oxidizing potentials, followed by reduction.

Synthesis of (($^{(S,S)\text{-}1,2\text{-}Cy,BMe_2}TC^{H}$)Fe(NMes), 2.

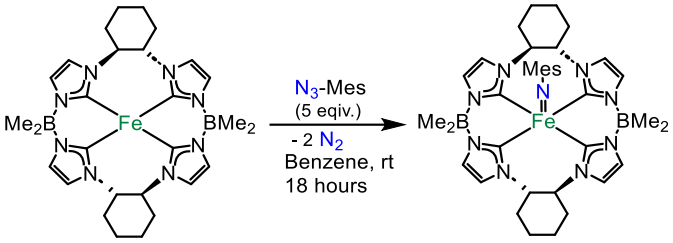

1 **2**

1 mL of a 35.33 mM solution of [($^{(S,S)\text{-}1,2\text{-}Cy,BMe_2}TC^{H}$)Fe], **1** (0.0035 mmol, 1 eq.) in benzene was added to a 20 mL scintillation vial. Mesityl azide 0.0284 g, 0.0177 mmol, 5 eq.) was then added to the vial as a 1 mL benzene solution. The reaction immediately evolved gas (N_2) and the solution turned a dark blue color. After 18 h of stirring at rt, a precipitate formed. This precipitate was filtered through a short Celite plug. The collected benzene was removed under reduced pressure and a dark blue solid was washed with hexanes (3 x 4 mL) to remove excess organic azide. The solid was then dried under reduced pressure yielding **2** as a blue powder (0.0129 g, 52.3% yield). Single crystals of **2** were grown by dissolving **2** in benzene (less than 1 mL) followed by layering ^{n}hexane at room temperature.

^{1}H NMR (499.74 MHz, C_6D_6): δ 279.19, 202.85, 85.51, 25.07, 8.64, 6.41, 4.07, 3.18, 2.94, 2.69, 2.45, 2.11, 2.02, 1.68, 1.26, 1.11, 0.86, -0.38, -11.31.

IR: 2928, 2657, 1736, 1450, 1426, 1398, 1292, 1261, 1230, 1210, 1038, 943, 833, 738, 694, 636 cm^{-1}

UV-Vis (THF): 366 nm (720 L/mol*cm).

Evans Method: 2.82 μ_B

LDI HR MS (m/z): $[M\text{-}Me]^+$: 684.3577 (found), $[C_{36}H_{48}B_2N_9Fe]^+$: 684.3568 (calculated)

Synthesis of ($^{(S,S)\text{-}1,2\text{-}Cy,BMe_2}TC^{H}$)Fe((*n*-octyl)$N_4$(*n*-octyl)), 3.

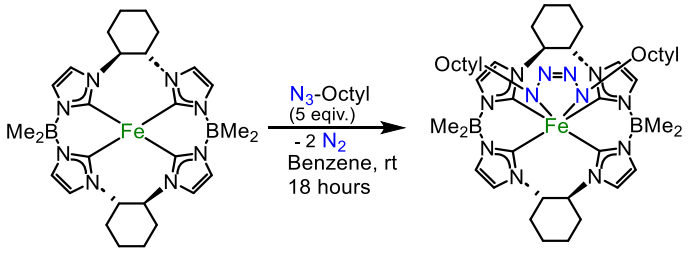

1 **3**

1 mL of a 35.33 mM solution of [($^{(S,S)\text{-}1,2\text{-}Cy,BMe_2}TC^{H}$)Fe], **1** (0.0035 mmol, 1 eq.) in benzene was added to a 20 mL scintillation vial. Octyl azide (0.0274 g, 0.0177 mmol, 5 eq.) was then added to the vial as a 1 mL benzene solution. The reaction immediately evolved gas (N_2) and the solution turned a dark red color. After 18 h of stirring at rt, the benzene was removed under reduced pressure and the red solid was washed with hexanes (3 x 4 mL) to remove excess organic azide. The solid was then dried under reduced pressure yielding **3** as a burgundy-colored powder (0.0230 g, 76% yield). Single crystals of **3** were grown by dissolving **3** in benzene (less than 1 mL) followed by vapor diffusion of pentane at room temperature.

^{1}H NMR (499.74 MHz, C_6D_6): δ 7.29 (s, 2H), 7.21 (s, 2H), 6.54 (s, 2H), 6.16 (s, 2H), 4.22 (td, J = 11.5, 4.2 H, 2H), 3.69 (td, J = 11.3, 5.0 Hz, 2H), 2.97 (dd, J = 17.1, 9.1 Hz, 2H), 2.11 (s, 2H), 1.63 (t, J = 7.6 Hz, 6H), 1.42-1.27 (m, 16H), 1.20 (s, 8H), 1.10 (s, 2H), 0.96 (m, 4H), 0.89 (t, J = 7.6 Hz, 6H), 0.80 (s, 6H), 0.73 (s, 2H), 0.67 (m, 2H), 0.22 (s, 6H).

^{13}C{^{1}H} NMR (125.66 MHz, C_6D_6): δ 171.26, 166.10, 124.80, 124.12, 123.57, 115.71, 66.90, 65.34, 54.19, 34.46, 32.13, 30.68, 29.83, 29.61, 29.52, 28.48, 25.08, 24.68, 23.08, 22.73, 14.35, 14.28.

IR: 2954, 2923, 2854, 2095, 1669, 1465, 1378, 1261, 1206, 1047, 802, 723, 691, 663 cm^{-1}

UV-Vis (THF): 362 nm (4400 mol^{-1} cm).

ESI HR MS (*m*/*z*): $[M+H]^+$: 849.5729 (found), $[C_{44}H_{75}B_2N_{12}Fe]^+$: 849.5773 (calculated)

Synthesis of ($^{(S,S)\text{-}1,2\text{-}Cy,BMe_2}TC^{H}$) Fe(N^{t}Butyl)$_2$, 4.**

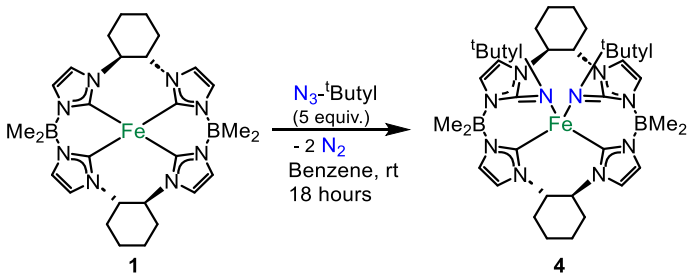

1 4

1 mL of a 35.33 mM solution of [($^{(S,S)\text{-}1,2\text{-}Cy,BMe_2}TC^{H}$)Fe], **1** (0.0035 mmol, 1 eq.) in benzene was added to a 20 mL scintillation vial. *Tert*-butyl azide (0.0175 g, 0.0177 mmol, 5 eq.) was then added to the vial as a 1 mL benzene solution. The reaction immediately evolved gas (N_2) and the solution turned a dark amber color. After 18 h of stirring at rt, the benzene was removed under reduced pressure and the red solid was washed with hexanes (3 x 4 mL) to remove excess organic azide. The solid was then dried under reduced pressure yielding **4** as a red powder (0.0159 g, 63.5% yield). Single crystals of **4** were grown by dissolving **4** in benzene (less than 1 mL) followed by layering hexane at room temperature.

^{1}H NMR (499.74 MHz, C_6D_6): δ 111.92, 58.87, 37.65, 31.75, 31.32, 24.43, 24.05, 22.78, 15.58, 15.39, 15.21, 14.61, 13.29, 11.49, 11.17, 10.96, 9.48, 6.08, 3.95, 3.39, 2.98, 2.67, 1.51, 1.31, 0.92, 0.65, 0.56, 0.01, -0.16, -11.18, -15.20, -16.73, -18.60, -20.07, -22.80, -36.71, -50.25, -75.10.

IR: 3136, 2933, 2863, 1538, 1449, 1414,1389, 1361, 1273, 1231,1169, 1033, 945, 913, 882, 793, 730, 661 cm^{-1}

UV-Vis: 365 nm (1300 L/mol*cm).

Evans Method: 3.14 μ_B

LDI-MS: $[M]^+$: 708.4358 (found), $[C_{36}H_{58}B_2N_{10}Fe]^+$: 708.4382 (calculated)

Synthesis of ($^{(S,S)\text{-}1,2\text{-}Cy,BMe_2}TC^{H}$) Fe(N-*p*-tolyl)$_2$), 5.**

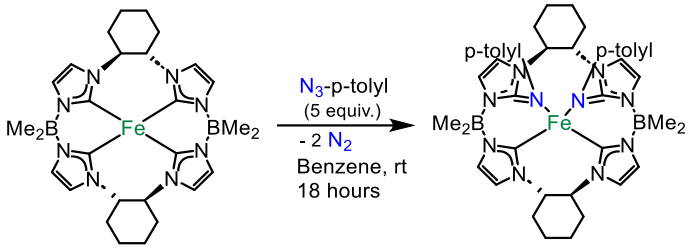

1 **5**

1 mL of a 35.33 mM solution of [($^{(S,S)\text{-}1,2\text{-}Cy,BMe_2}TC^{H}$)Fe], **1** (0.0035 mmol, 1 eq.).) in benzene was added to a 20 mL scintillation vial. *p*-Tolyl azide (0.0175 g, 0.0177 mmol, 5 eq.) was then added to the vial as a 1 mL benzene solution. The reaction immediately evolved gas (N_2) and the solution turned a dark yellow-green color. After 18 h of stirring at rt, a precipitate formed. This precipitate was filtered through a short Celite plug. The collected benzene was removed under reduced pressure and the dark yellow solid left was washed with hexanes (3 x 4 mL) to remove excess organic azide. The solid was then dried under reduced pressure yielding a yellow powder. Single crystals of **5** were grown by dissolving **5** in benzene (less than 1 mL) followed by layering ^{n}hexane at room temperature and a single crystal was picked elucidating **5**. However, NMR and other spectrochemical analysis could not be obtained due to poor purity and yield of **5**.

Attempted Catalytic Reactions:

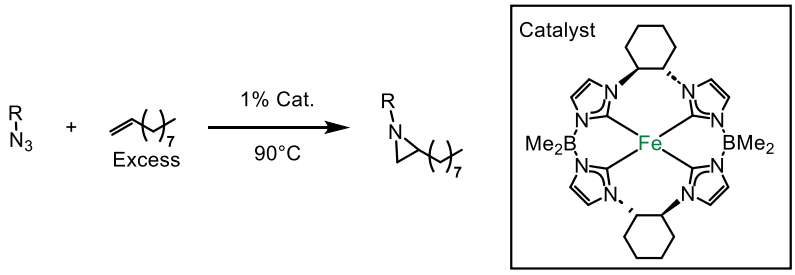

[($^{(S,S)\text{-}1,2\text{-}Cy,BMe2}TC^{H}$)Fe] (**1**) was added to a 20 mL vial followed by the addition of 1-decene. The reaction mixture was heated to 90 °C and stirred for 10 min. The organic azide was then added to the reaction as a 1-decene solution, which was then stabilized to the designated temperature. Once the organic azide was no longer present (as determined by TLC/ DART-MS) the mixture was removed from heat, and this crude product was purified by column chromatography on silica gel using a gradient elution of a mixture of ethyl acetate and hexanes.[6] The corresponding excess alkene can be recovered from the column as it comes out with pure hexanes as eluent.

Attempted synthesis of 2-octyl-1-(mesityl)aziridine, 6.

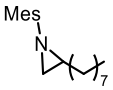

Mesityl azide (0.083 g, 0.53 mmol) and 1-decene (3.78 g, 5.02 mL) were used in the General Catalytic Reaction described above and at 1% catalyst loading, but no aziridine was formed with **1**.

Attempted synthesis of 1,2-dioctylaziridine, 7.

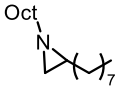

Octyl azide (0.082 g, 0.53 mmol) and 1-decene (3.78 g, 5.02 mL) were used in the General Catalytic Reaction described above and at 1% catalyst loading, but no aziridine was formed with **1**.

Attempted synthesis of 1-(tert-butyl)-2-octylaziridine, 8.

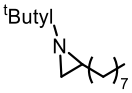

Tert-butyl azide (0.052 g, 0.53 mmol) and 1-decene (3.78 g, 5.02 mL) were used in the General Catalytic Reaction described above and at 1% catalyst loading, but no aziridine was formed with **1**.

Spectra and other analytical data for isolated compounds

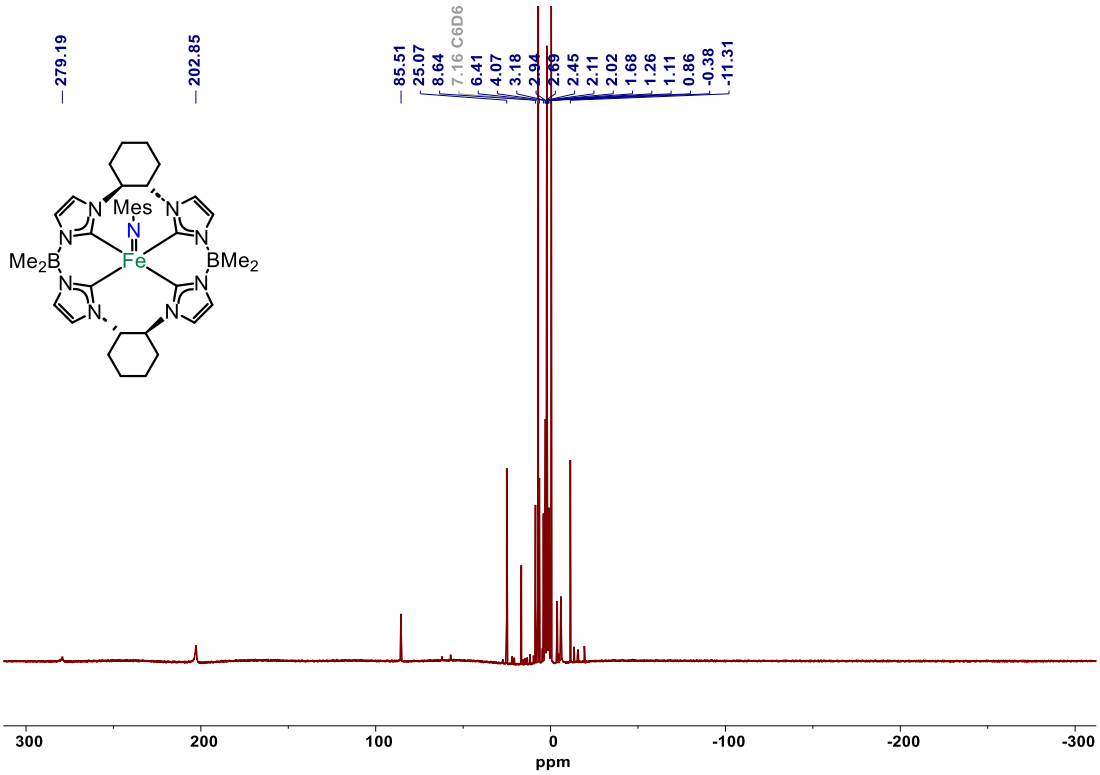

Figure S1. ^{1}H NMR of **2** in C_6D_6.

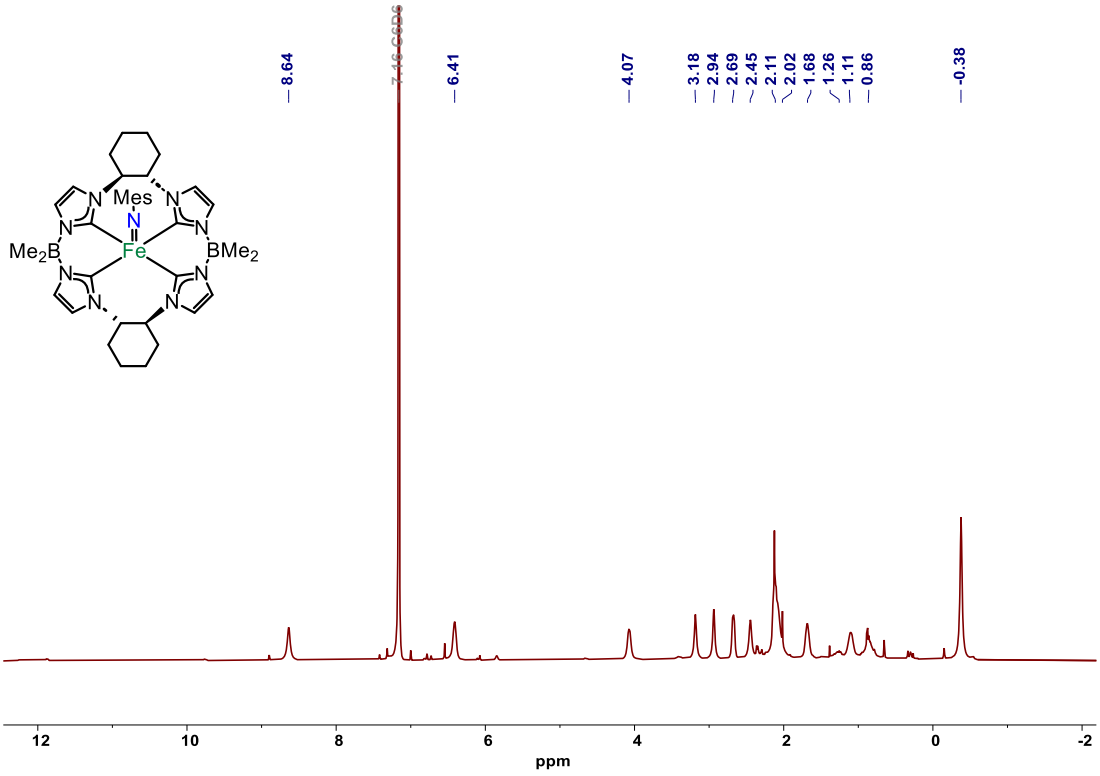

Figure S2. ^{1}H NMR Diamagnetic Region of **2** in C_6D_6.

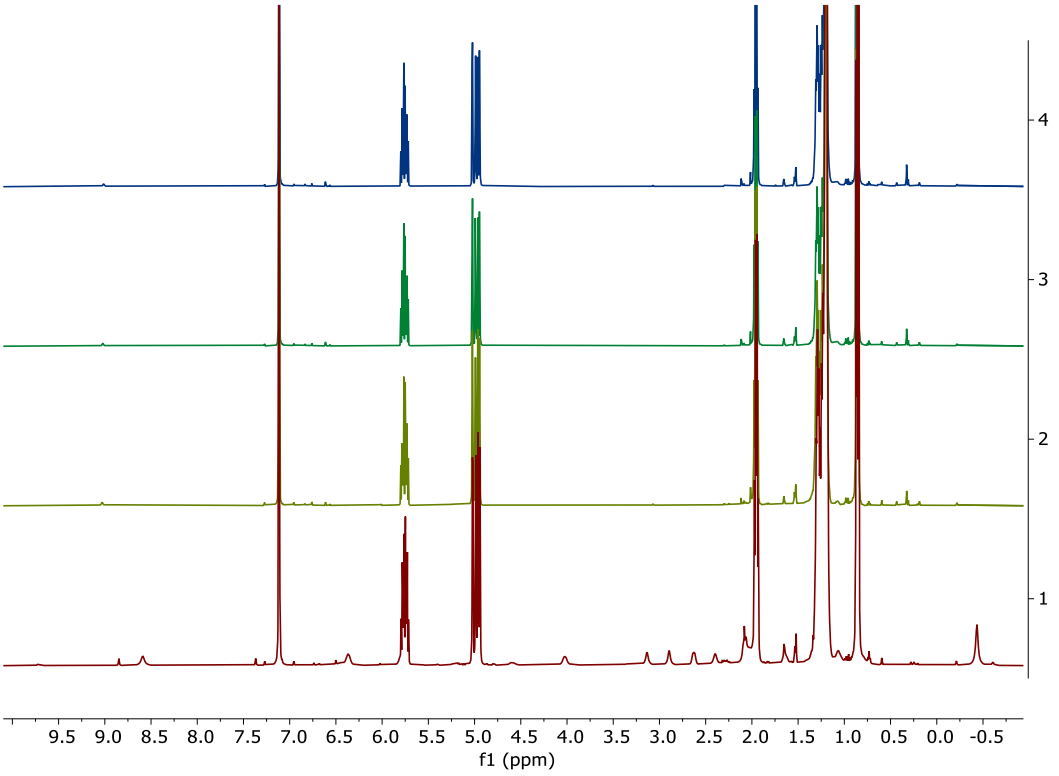

Figure S3. ^{1}H NMR of **2** in C_6D_6 reacted with 1-decene at 80 °C for 72 hrs.

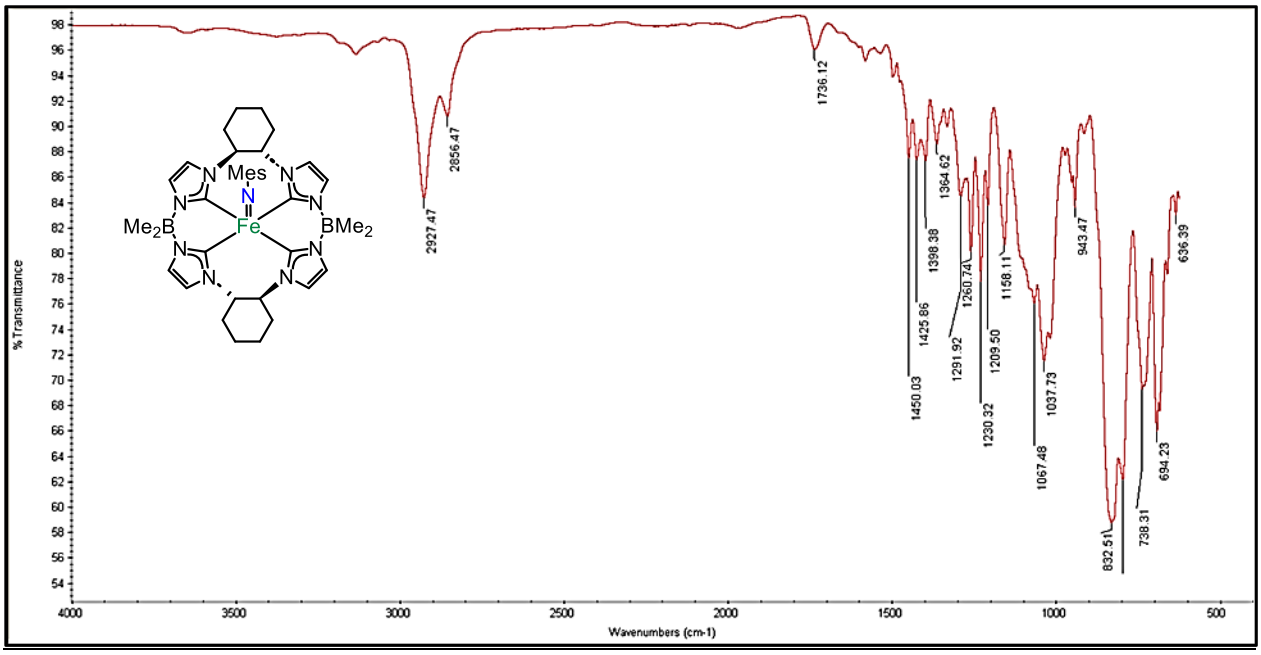

Figure S4. IR of **2**.

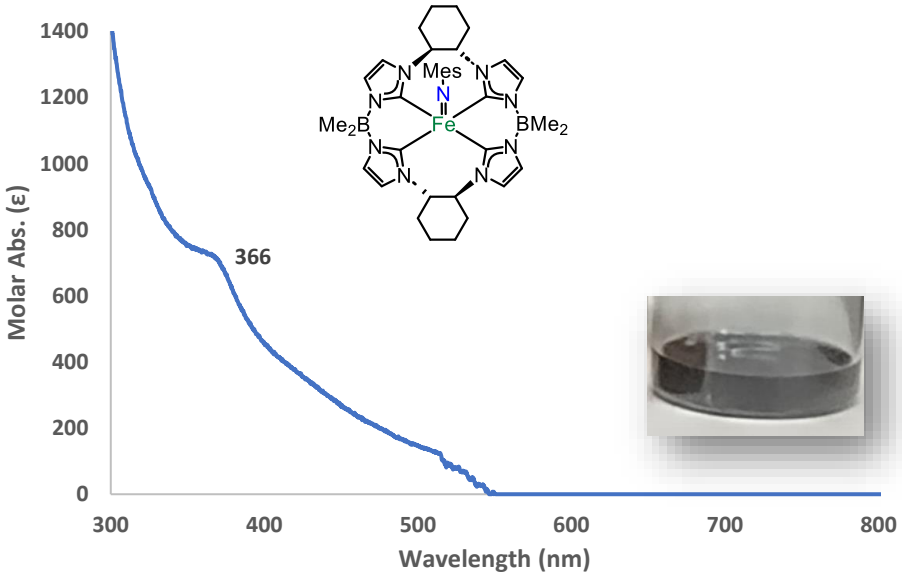

Figure S5. UV-Vis spectrum of **2** in THF.

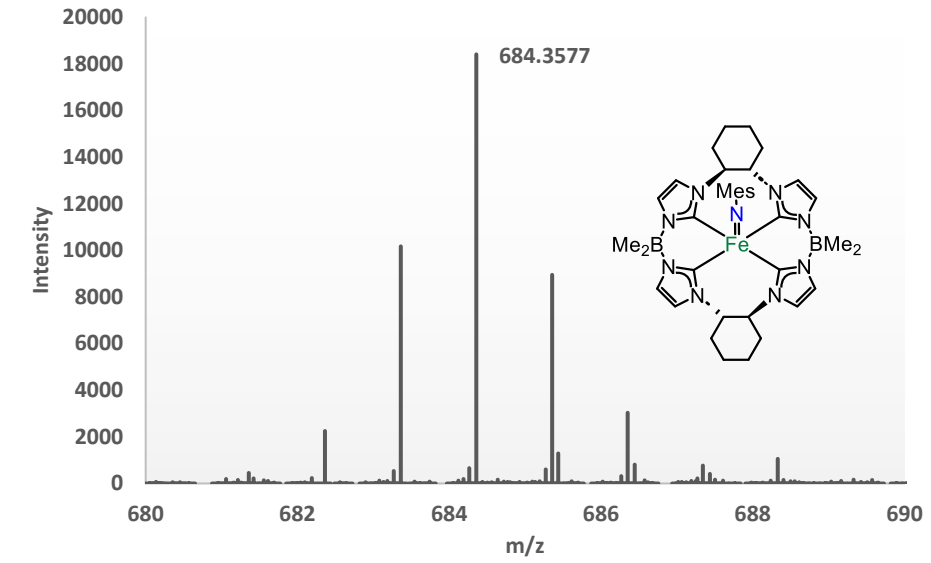

Figure S6. HR LDI-MS of **2**.

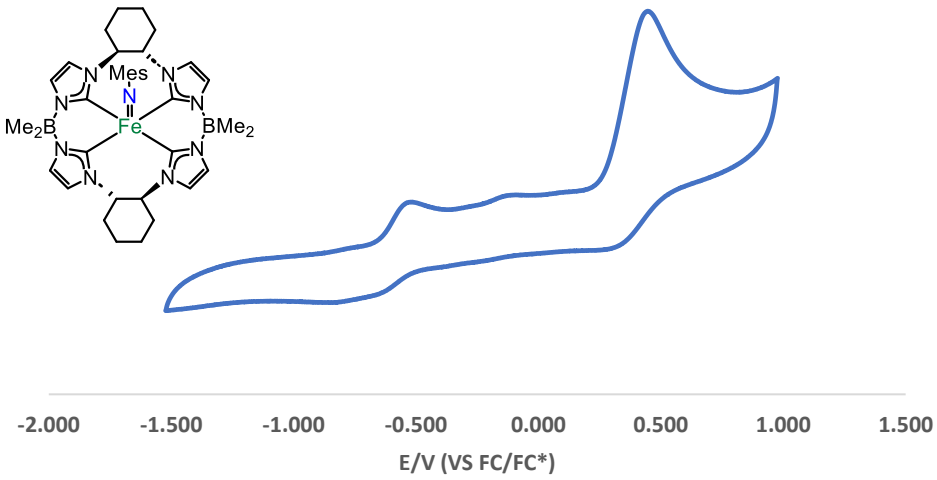

Figure S7. Cyclic voltammogram of **2** in CH_3CN at 50 mV/s scan rate.

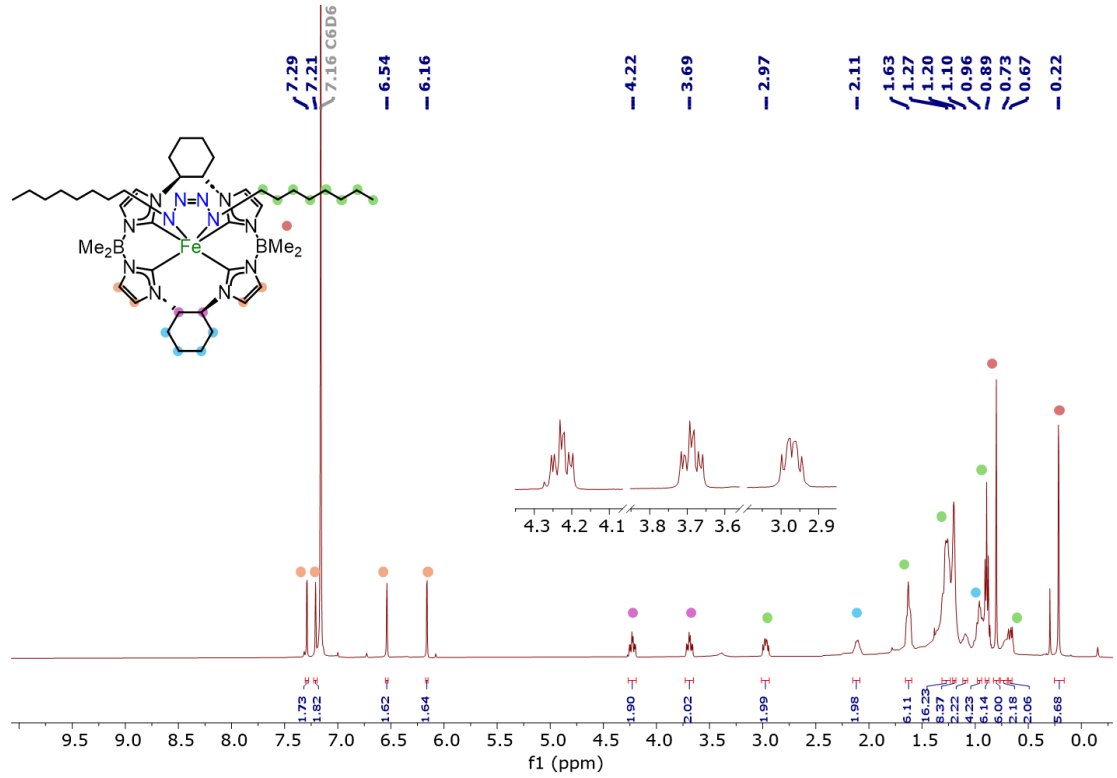

Figure S8. ^{1}H NMR of **3** in C_6D_6.

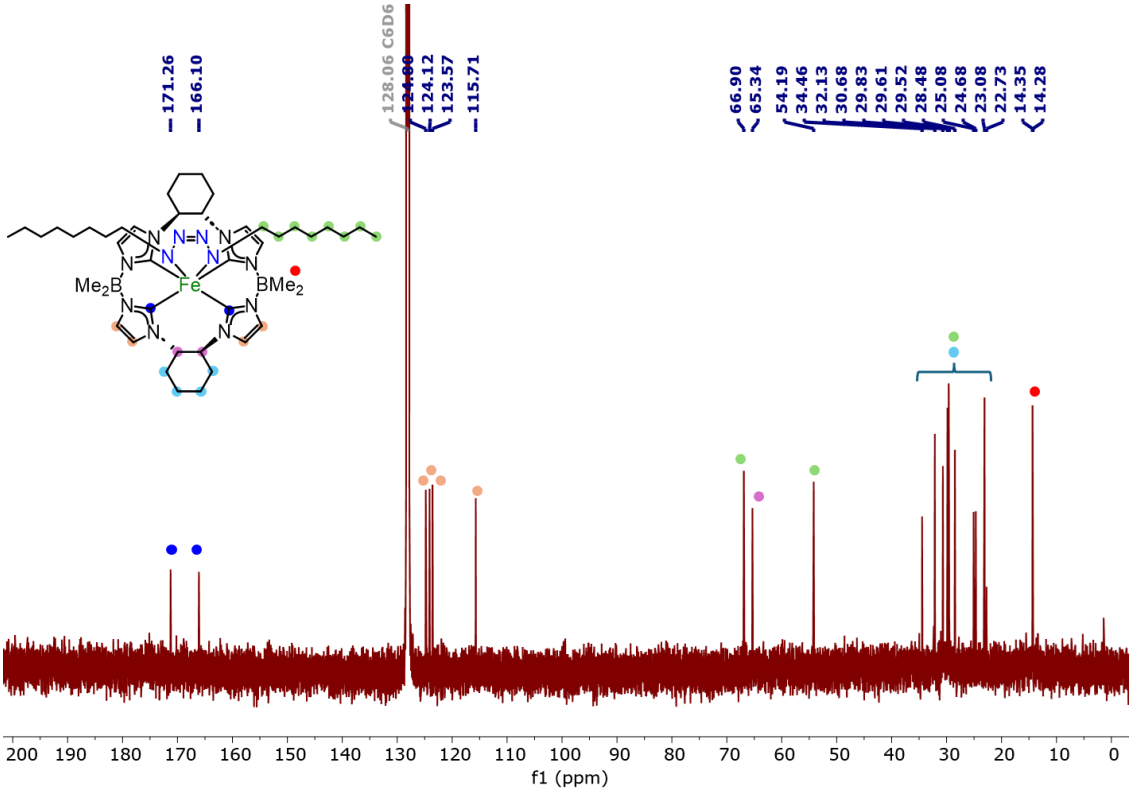

Figure S9. ^{13}C NMR of **3** in C_6D_6.

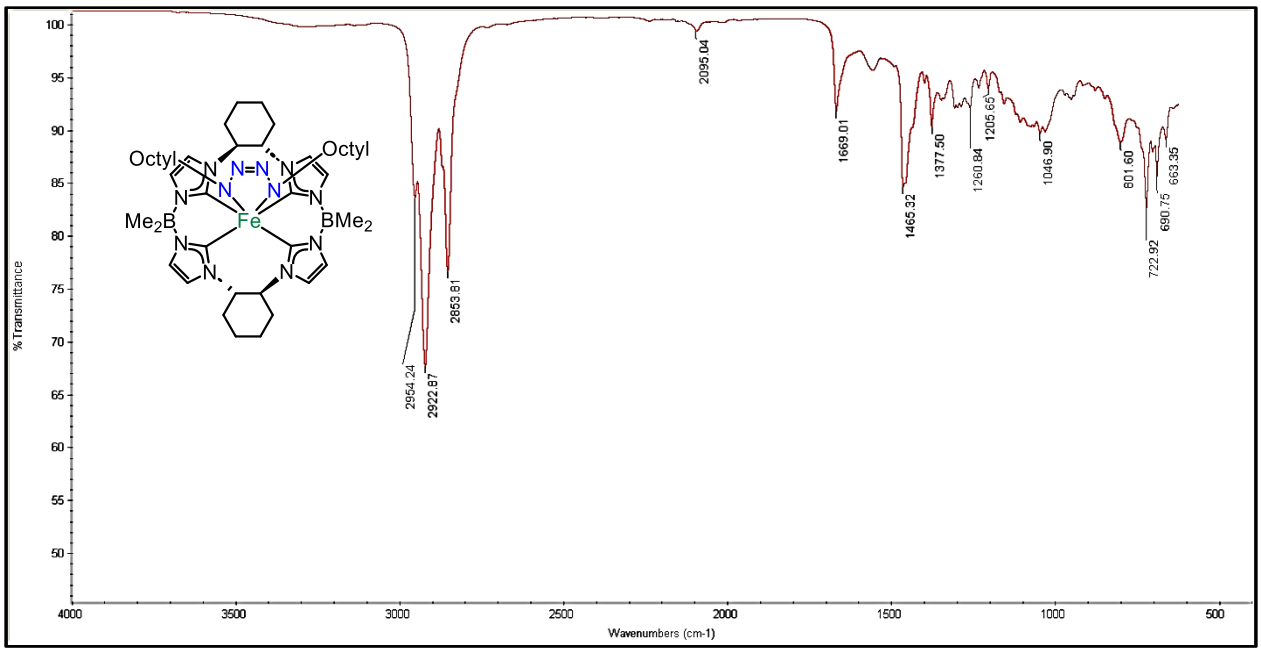

Figure S10. IR spectrum of **3**.

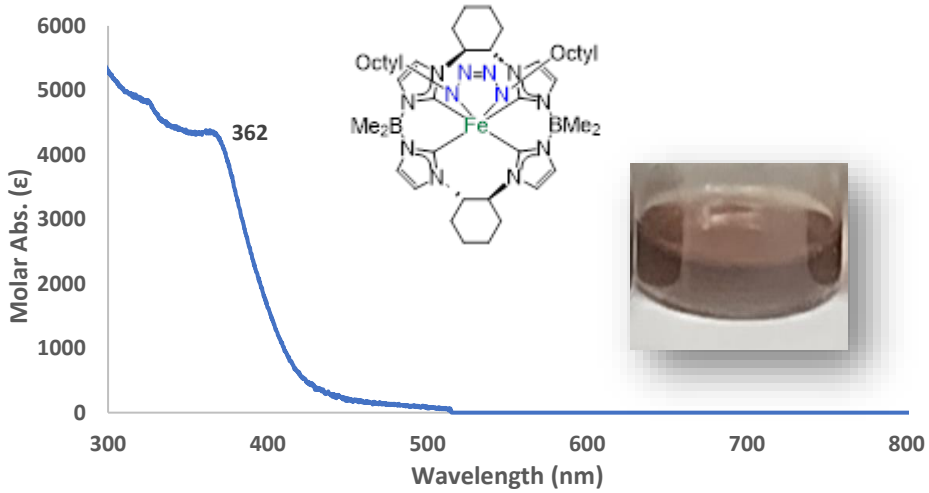

Figure S11. UV-Vis spectrum of **3** in THF.

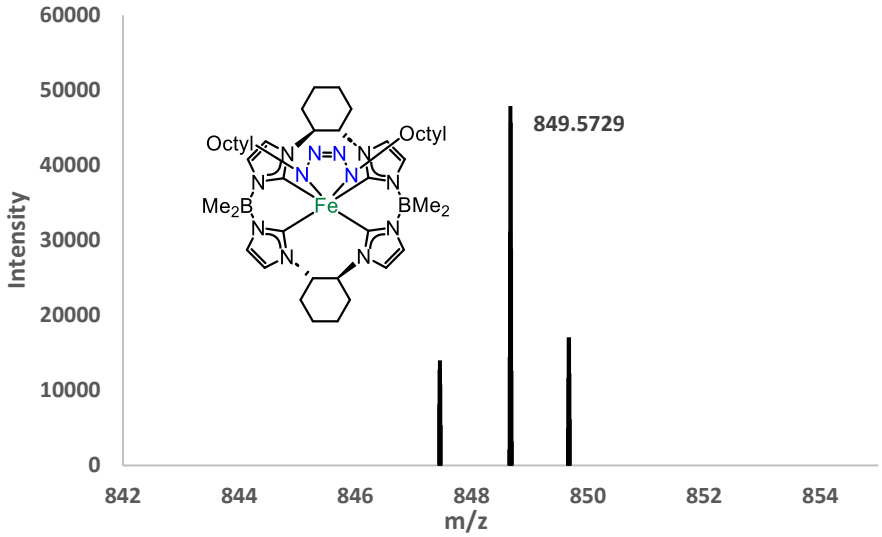

Figure S12. HR ESI-MS of **3**.

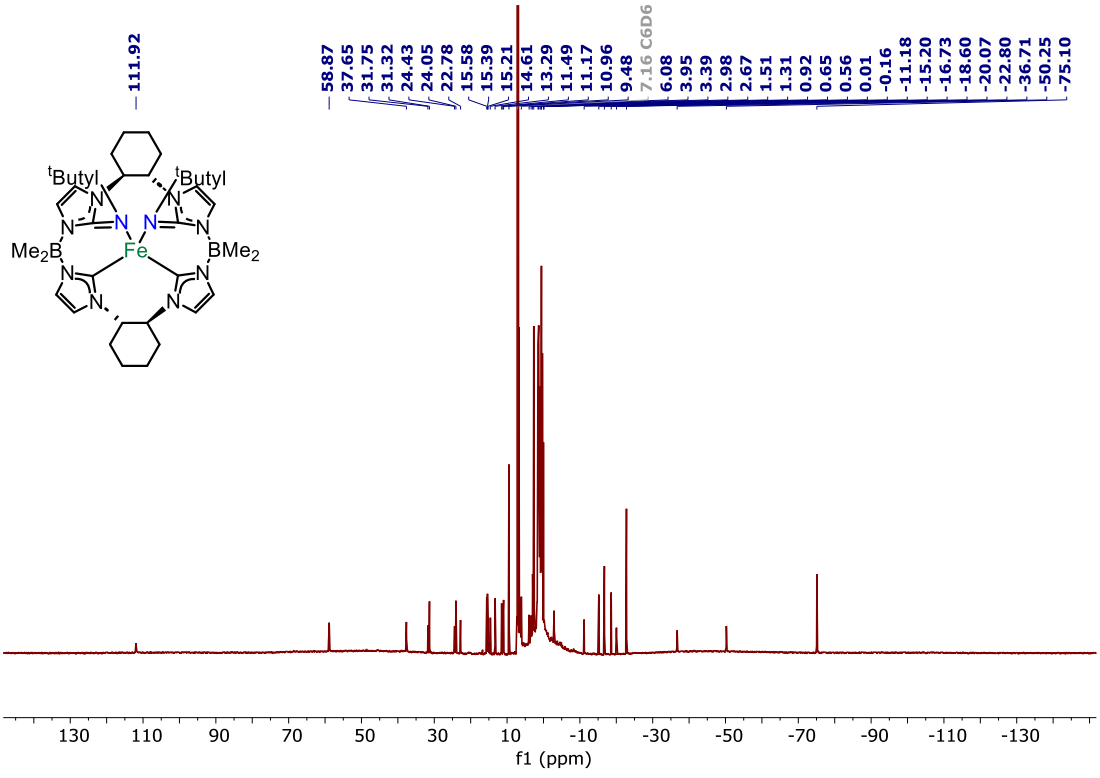

Figure S13. ^{1}H NMR of **4** in C_6D_6.

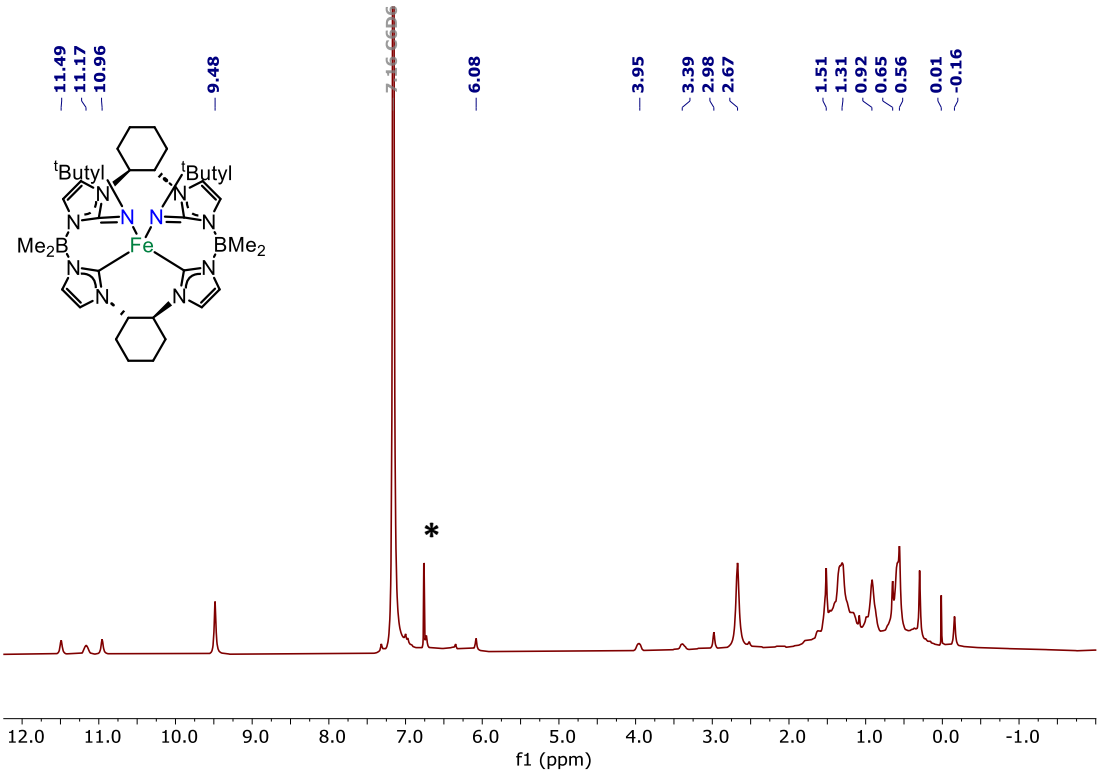

Figure S14. ^{1}H NMR Diamagnetic Region of **4** in C_6D_6.

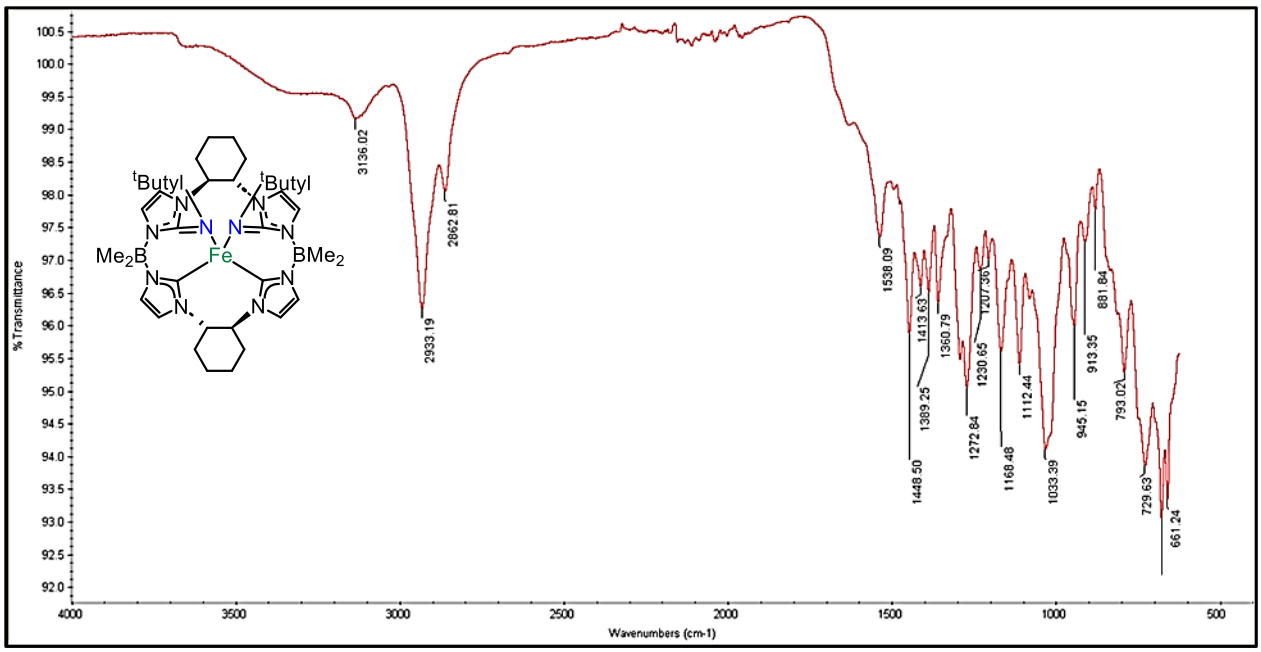

Figure S15. IR of **4**.

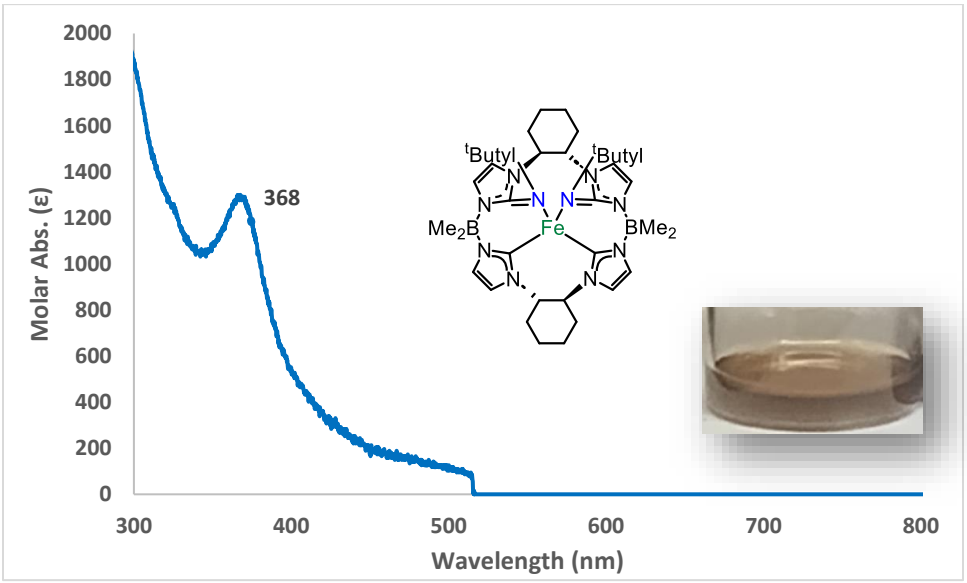

Figure S16. UV-Vis spectrum of **4** in THF.

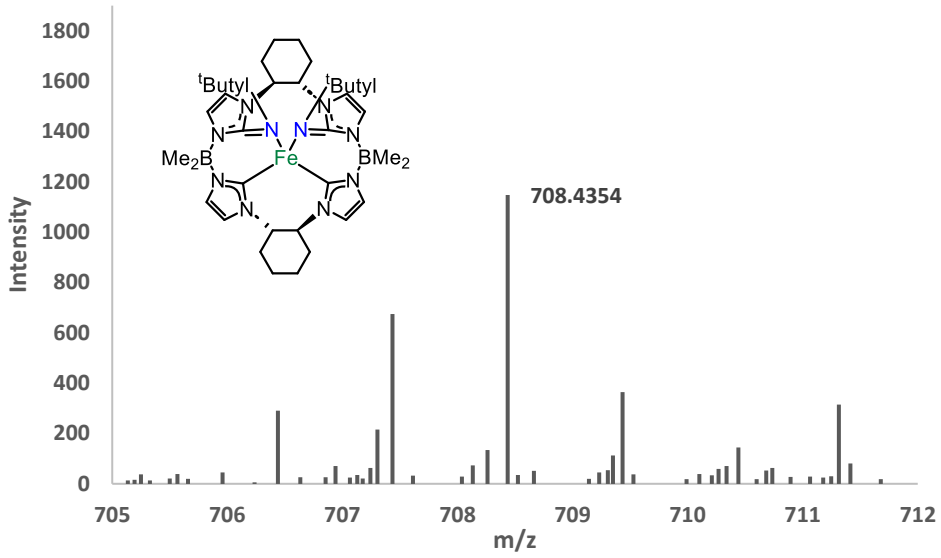

Figure S17. HR LDI-MS of **4**.

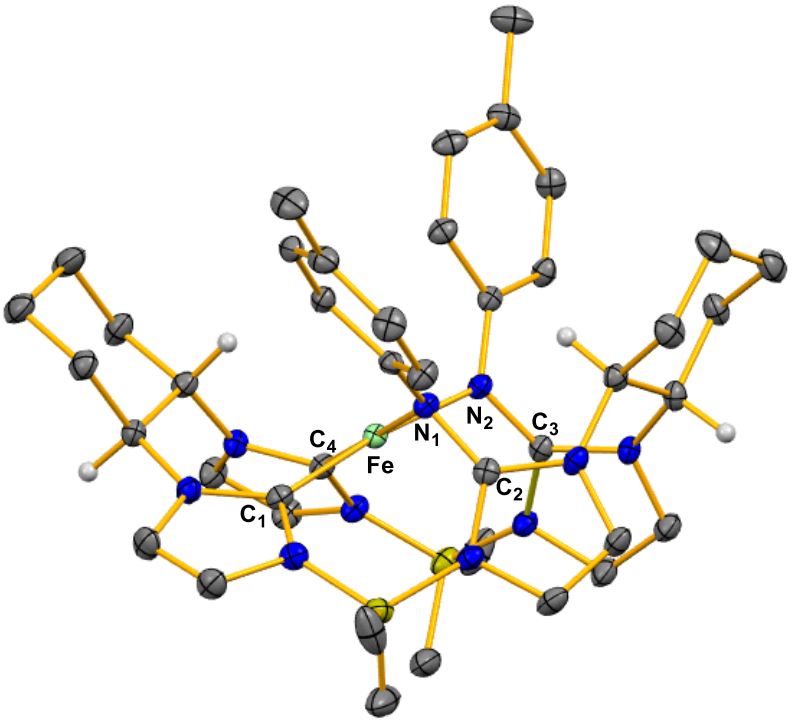

Figure S18. The molecular structure of **5** as determined by single crystal X-ray diffraction. Green, blue, gray, olive, and white ellipsoids (50% probability) represent Fe, N, C, B, and H atoms, respectively. Solvent molecules and H-atoms on non-stereogenic atoms are omitted for clarity.

Computational methods

All geometry optimizations and frequency calculations were carried using the ORCA 5.0.2 software package.[7] All results shown herein were obtained with the PBE density functional, along with Grimme's D3 dispersion correction with Becke-Johnson Damping (D3(BJ)) and the resolution of identity (RI).[8-11] The def2-SVP basis set was used for all non-iron atoms, while iron employed the def2-TZVP basis set, with matching auxiliary basis sets.[12] The choice of the PBE-D3(BJ)/def2-TZVP(Fe),def2-SVP(C,N,H) level was based on a previous computational study on the catalytic aziridination with a similar Fe-tetracarbene complex.[13] Transition states were optimized using a combination of relaxed surface scans and a subsequent transition state optimization algorithm of ORCA 5.0.2. Transition states involving insertion (**TS1** and **TS2**) the carbene-iron-imide angle was scanned from approximately 100° to 40° (shown in figure below). Transition states forming metallotetrazene utilized the transition state optimization algorithm only. Coordinates for all intermediates and transition states can be found in a separate text file.

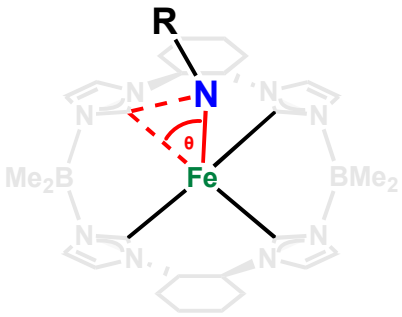

Figure S19. Scheme of the transition state mode for insertion to NHC macrocycle

Computations figures and tables

	Spin	E (E_h)	G (E_h)	ΔG_{spin} (kcal/mol)	$\Delta G_{reaction}$ (kcal/mol)
N_2	0	-109.3217372	-109.3347444		
FeL (**1**)	1	-2839.475424	-2838.884959	0	
	2	**-2839.413346**	**-2838.825413**	37.4	
t-Butyl azide	0	-321.429899	-321.330577		
A - Fe-azide	0	-3160.907846	-3160.188416	12.6	
	1	**-3160.922502**	**-3160.208466**	0	**4.4**
	2	-3160.904982	-3160.188836	12.3	
TS1	1	-3160.908890	-3160.194638		**13.1**
B - imide	**0**	**-3051.650234**	**-3050.937497**	**0**	**-35.6**
	1	-3051.639408	-3050.92984	4.8	
	2	-3051.608769	-3050.902685	21.8	
TS2 - tetrazene formation	**0**	**-3373.092847**	**-3372.252858**	**0**	**-26.0**
	1	-3373.075301	-3372.217117	22.4	
C -metalotetrazene	0	-3373.133340	-3372.288193	0	**-48.2**
	1	-3373.104126	-3372.263573	15.4	
	2	-3373.077944	-3372.243723	27.9	
TS3 - insertion	**1**	**-3051.614715**	**-3050.904995**		**-15.2**
D - insertion	**1**	**-3051.660212**	**-3050.949108**	**0**	**-42.9**
	2	-3051.624161	-3050.91539	21.2	
TS4 - 2nd insertion	0	-3263.791033	-3262.960774	6.4	
	1	**-3263.800239**	**-3262.970956**	**0**	**-59.2**
	2	-3263.761126	-3262.935154	22.5	
E - 2nd insertion (**4**)	0	-3263.830537	-3263.000445	11.1	
	1	**-3263.847026**	**-3263.018135**	**0**	**-88.8**
	2	-3263.806233	-3262.981657	22.9	
Mesityl azide	0	-512.8159327	-512.6717235		
A - Fe-azide	**1**	**-3352.320702**	**-3351.559398**	**0**	**-1.7**
	2	-3352.299365	-3351.537075	14.0	
TS1	**1**	**-3352.303968**	**-3351.543765**	**0**	**8.1**
	2	-3352.296616	-3351.533871	6.2	
B – imide (**2**)	0	-3243.059644	-3242.302944	4.4	
	1	**-3243.063316**	**-3242.309929**	**0**	**-55.2**
	2	-3243.041204	-3242.290683	12.1	
TS2 - tetrazene formation	**0**	**-3755.849148**	**-3754.915495**	**0**	**-13.7**
	1	-3755.844102	-3754.914733	0.5	
C -metalotetrazene	**0**	**-3755.872754**	**-3754.935163**	**0**	**-26.0**
	1	-3755.857835	-3754.92374	7.2	
	2	-3755.857569	-3754.93016	3.1	
TS3 - insertion	**0**	**-3243.016816**	**-3242.262828**	**0**	**-25.7**
	1	-3242.99301	-3242.241012	13.7	
D - insertion	**1**	**-3243.053524**	**-3242.300108**	**0**	**-49.1**
	2	-3243.023721	-3242.270965	18.3	

Octyl azide	0	-478.3477837	-478.1449561		
A - Fe-azide	0	-3317.840689	-3317.020451	7.5	
	1	**-3317.850401**	**-3317.032338**	**0**	**-1.5**
	2	-3317.835331	-3317.016752	9.8	
TS1	1	-3317.840804	-3317.02364		**3.9**
B – imide	**0**	**-3208.570545**	**-3207.75624**	**0**	**-38.3**
	1	-3208.563322	-3207.751095	3.2	
	2	-3208.53223	-3207.722547	21.1	
TS2 - tetrazene formation	0	-3686.942773	-3685.896267		**-35.2**
C -metalotetrazene (**3**)	**0**	**-3687.010125**	**-3685.957853**	**0**	**-73.9**
	1	-3686.984547	-3685.935816	13.8	
	2	-3686.946237	-3685.900696	35.9	
TS3 - insertion	**1**	**-3208.520594**	**-3207.709915**	**0**	**-9.3**
	2	-3208.499306	-3207.689699	12.7	
D - insertion	**1**	**-3208.572671**	**-3207.758375**	**0**	**-39.7**
	2	-3208.542363	-3207.730621	17.4	

DFT optimized geometries compared to X-Ray crystal structures

All distances in Å, all angles in degrees.

Mesityl Imide (2) – S = 1

	DFT	Exp	Diff
Fe-N	1.707	1.759	0.052
		1.73	0.023
Average			**0.038**
Fe-C(1)	1.945	2.003	0.058
		1.991	0.046
Fe-C(2)	1.941	1.969	0.028
		1.993	0.052
Fe-C(3)	2.031	2.025	0.006
		2.041	0.01
Fe-C(4)	1.988	1.982	0.006
		1.975	0.013
Average			**0.027**
Fe-N-C	160.7	162.2	1.5
		162.7	2
Average			**1.8**
C-C-C-C	-14.5	-3.7	10.8
		-4.5	10
Average			**10.4**

Octyl Tetrazene (3) – S = 0

	DFT	Exp	Diff
Fe-N(1)	1.893	1.880	0.013
Fe-N(2)	1.897	1.887	0.010
Average			**0.012**
Fe-C(1)	2.023	2.024	0.001
Fe-C(2)	1.976	1.991	0.015
Fe-C(3)	2.013	2.015	0.002
Fe-C(4)	1.973	1.986	0.013
Average			**0.008**
C-C-C-C	-14.831	-13.6	1.231
N-N-N-N	-3.119	-3.2	0.081

Tert-Butyl Bis-insertion (4) – S = 1

	DFT	Exp	Diff
Fe-N(1)	1.945	1.995	0.050
		1.964	0.019
Fe-N(2)	1.983	2.029	0.046
		2.014	0.031
Average			**0.037**
Fe-C(1)	1.971	1.991	0.02
		1.989	0.018
Fe-C(2)	1.933	1.947	0.014
		1.954	0.021
Average			**0.018**
N-Fe-N	99.3	96.4	2.9
		94.9	4.4
Average			**3.7**
C-C-N-N	-6.3	-6.1	0.2
		-2.6	3.7
Average			**2.0**

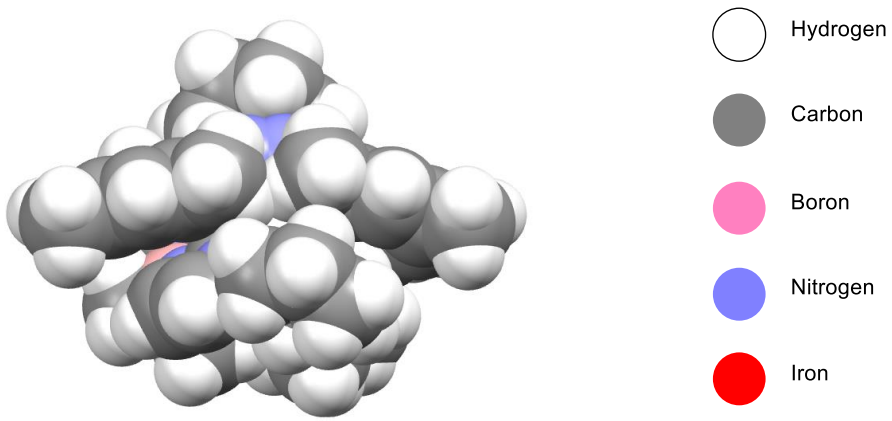

Figure S20. Space filling model for mesityl azide reaction with iron imide going to TS_2 as shown in Fig. 3 in main text. Representation is shown as a side view.

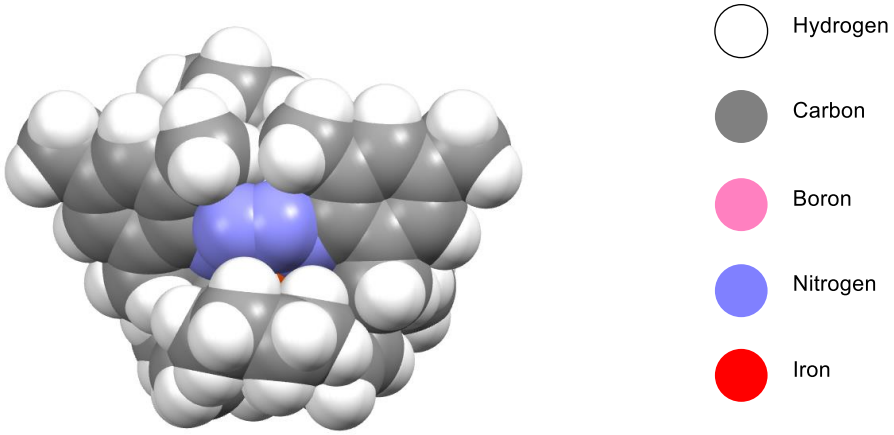

Figure S21. Space filling model for mesityl azide reaction with iron imide going to TS_2 as shown in Fig. 3 in main text. Representation is shown as a top view.

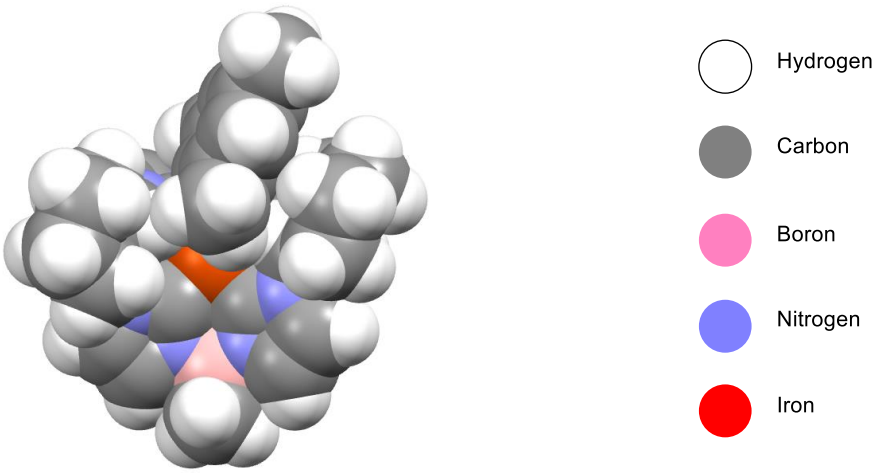

Figure S22. Space filling model for mesityl azide reaction with iron imide going to TS_3 as shown in Fig. 3 in main text. Representation is shown as a top view.

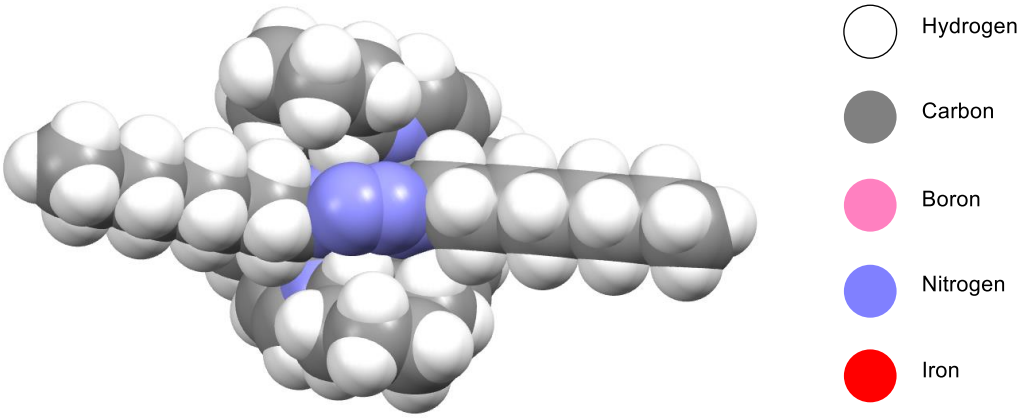

Figure S23. Space filling model for octyl azide reaction with iron imide going to TS_2 as shown in Fig. 3 in main text. Representation is shown as a top view.

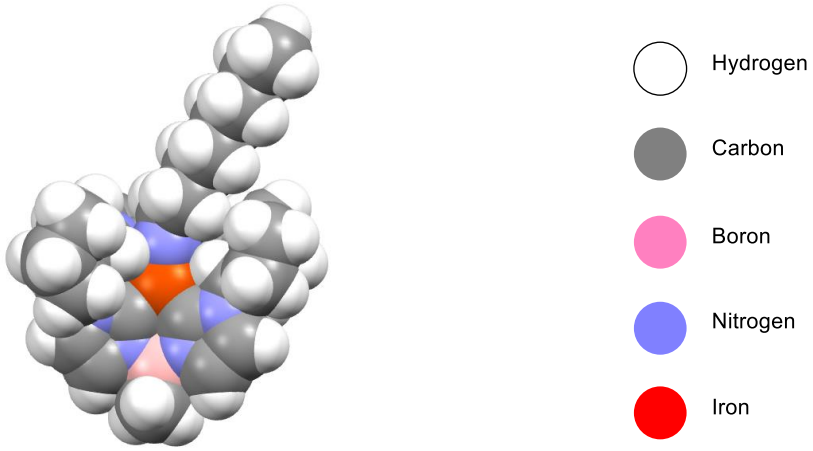

Figure S24. Space filling model for octyl azide reaction with iron imide going to TS_3 as shown in Fig. 3 in main text. Representation is shown as a top view.

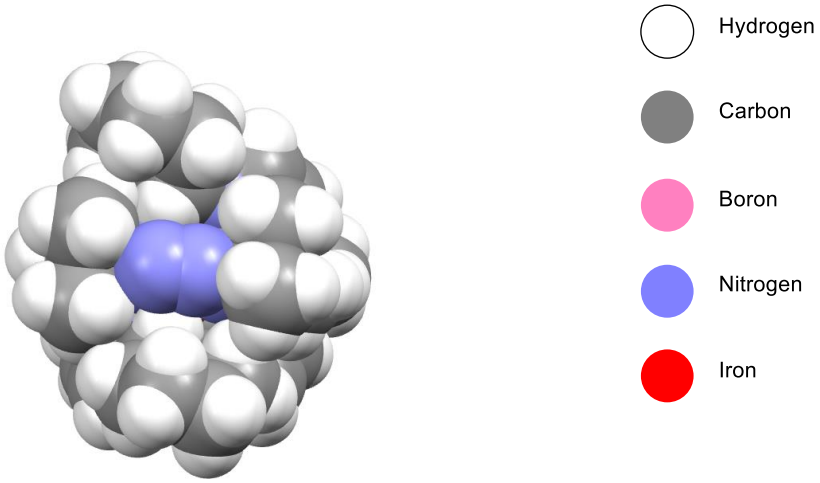

Figure S25. Space filling model for *tert*-butyl azide reaction with iron imide going to TS_2 as shown in Fig. 3 in main text. Representation is shown as a top view.

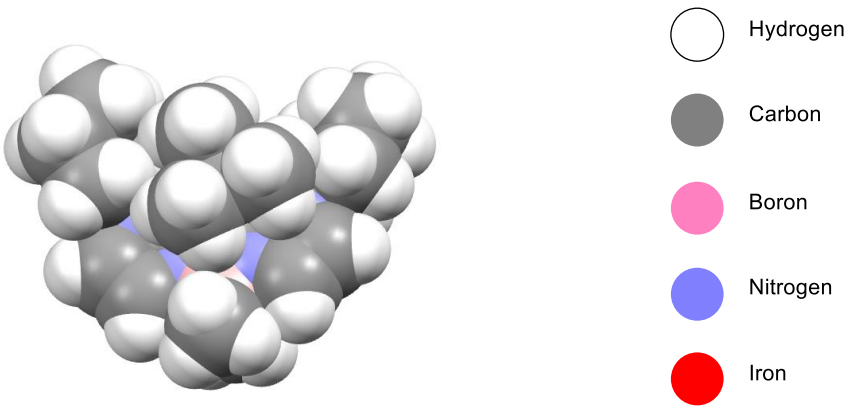

Figure S26. Space filling model for *tert*-butyl azide reaction with iron imide going to TS_3 as shown in Fig. 3 in main text. Representation is shown as a side view.

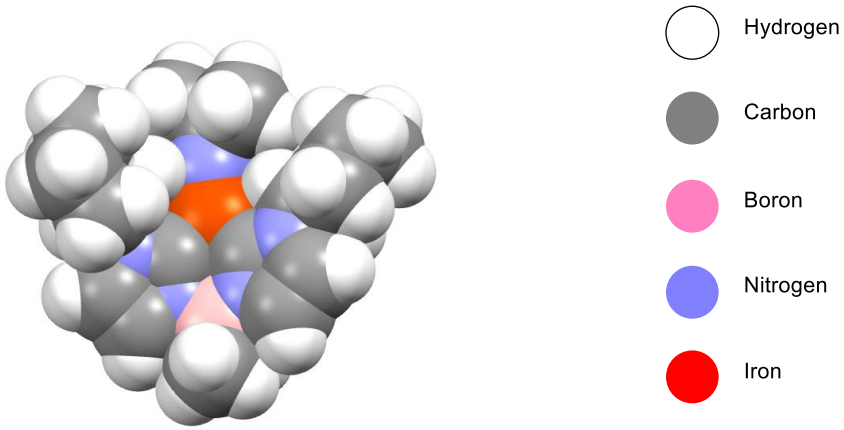

Figure S27. Space filling model for *tert*-butyl azide reaction with iron imide going to TS_3 as shown in Fig. 3 in main text. Representation is shown as a top view.

References

1. S. Alvarez* and M. Alvarez, *Synthesis*, 1997, **1997**, 413-414.
2. J. C. Bottaro, P. E. Penwell and R. J. Schmitt, *Synthetic Communications*, 1997, **27**, 1465-1467.
3. F. Kloss, U. Köhn, B. O. Jahn, M. D. Hager, H. Görls and U. S. Schubert, *Chemistry – An Asian Journal*, 2011, **6**, 2816-2824.
4. P. A. S. Smith and B. B. Brown, *Journal of the American Chemical Society*, 1951, **73**, 2438-2441.
5. J. F. DeJesus and D. M. Jenkins, *Chemistry – A European Journal*, 2020, **26**, 1429-1435.
6. P. P. Chandrachud, H. M. Bass and D. M. Jenkins, *Organometallics*, 2016, **35**, 1652-1657.
7. F. Neese, *WIREs Computational Molecular Science*, 2022, **12**, e1606.
8. J. P. Perdew, *Physical Review B*, 1986, **34**, 7406-7406.
9. S. Grimme, J. Antony, S. Ehrlich and H. Krieg, *The Journal of Chemical Physics*, 2010, **132**, 154104.
10. S. Grimme, S. Ehrlich and L. Goerigk, *Journal of Computational Chemistry*, 2011, **32**, 1456-1465.
11. F. Furche, R. Ahlrichs, C. Hättig, W. Klopper, M. Sierka and F. Weigend, *WIREs Computational Molecular Science*, 2014, **4**, 91-100.
12. F. Weigend and R. Ahlrichs, *Physical Chemistry Chemical Physics*, 2005, **7**, 3297-3305.
13. S. B. Isbill, P. P. Chandrachud, J. L. Kern, D. M. Jenkins and S. Roy, *ACS Catalysis*, 2019, **9**, 6223-6233.